J|A|C|S
ARTICLES
Published on Web 12/10/2005

Photoinduced Magnetization in Copper Octacyanomolybdate

Shin-ichi Ohkoshi,*[,†,‡] Hiroko Tokoro,[†] Toshiya Hozumi,[†] Yue Zhang,[†] Kazuhito Hashimoto,*[,†] Corine Mathonière,*[,§] Isabelle Bord,[§] Guillaume Rombaut,[§] Marc Verelst,[||] Christophe Cartier dit Moulin,[⊥,#] and Françoise Villain[⊥,#]

Contribution from the Department of Applied Chemistry, School of Engineering, The University of Tokyo, 7-3-1 Hongo, Bunkyo-ku, Tokyo 113-8656, Japan, PRESTO, JST, 4-1-8 Honcho Kawaguchi, Saitama 332-0012, Japan, ICMCB, CNRS UPR 9048, University of Bordeaux 1, avenue du Docteur Schweitzer, 33608 Pessac Cedex, France, CEMES, CNRS UPR 8011, BP 4743, 29 rue Jeanne Marvig, 31055 Toulouse Cedex, France, Laboratoire de Chimie Inorganique et Matériaux Moléculaires, UMR CNRS 7071, Université Paris 6, 4 place Jussieu, 75252 Paris Cedex 05, France, and LURE, Bât. 209D, Université Paris-Sud, BP34, 91898 Orsay Cedex, France

Received August 26, 2005; E-mail: ohkoshi@light.t.u-tokyo.ac.jp

Abstract: This article describes the studies of a photomagnetic cyanide-bridged Cu−Mo bimetallic assembly, $Cu^{II}_2[Mo^{IV}(CN)_8]\cdot 8H_2O$ (Cu^{II}, $S = {}^1/_2$; Mo^{IV}, $S = 0$) (**1**), which has an intervalence transfer (IT) band from $Mo^{IV}-CN-Cu^{II}$ to $Mo^{V}-CN-Cu^{I}$ around 480 nm. Wide-angle X-ray scattering and X-ray spectroscopic studies provide precise information about the 3D connectivity and the local environment of the transition metal ions. Irradiating with blue light causes solid **1** to exhibit a spontaneous magnetization (Curie temperature = 25 K). The thermal reversibility is carefully studied and shows the long-time stability of the photoinduced state up to 100 K. Photoreversibility is also observed; i.e., the magnetization is induced by irradiation with light below 520 nm, while the magnetization is reduced by irradiation with light above 520 nm. The UV−vis absorption spectrum after irradiation shows a decrease of the IT band and the appearance of the reverse-IT band in the region of 600−900 nm ($\lambda_{max} = 710$ nm). This UV−vis absorption spectrum is recovered to the original spectrum by irradiation with 658-, 785-, and 840-nm light. In this photomagnetic effect, the excitation of the IT band causes an electron transfer from Mo^{IV} to Cu^{II}, producing a ferromagnetic mixed-valence isomer of $Cu^{I}Cu^{II}[Mo^{V}(CN)_8]\cdot 8H_2O$ (Cu^{I}, $S = 0$; Cu^{II}, $S = {}^1/_2$; Mo^{V}, $S = {}^1/_2$) (**1′**). **1′** returns to **1** by irradiation of the reverse-IT band, which obeys the scheme for the potential energy surface in mixed-valence class II compounds.

1. Introduction

Over the past 15 years, Prussian blue analogues that involve hexacyanometalate $[M(CN)_6]^{n-}$ with 3d metal ions have been used to design and synthesize new molecular-based magnets due to their high critical temperatures and interesting functionalities.[1−5] Recently, polycyanides with higher coordination numbers have also attracted increasing attention. For example, the anisotropic magnetic effects on bimetallic cyanides of heptacyanomolybdate $[Mo(CN)_7]^{4-}$ were reported.[6] Moreover, high-

[†] The University of Tokyo.
[‡] PRESTO, JST.
[§] University of Bordeaux 1.
[||] CEMES, CNRS UPR 8011.
[⊥] Université Paris 6.
[#] Université Paris-Sud.

(1) (a) Verdaguer, M.; Bleuzen, A.; Marvaud, V.; Vaissermann, J.; Seuleiman, M.; Desplanches, C.; Scuiller, A.; Train, C.; Garde, R.; Gelly, G.; Lomenech, C.; Rosenman, I.; Veillet, P.; Cartier dit Moulin, C.; Villain, F. *Coord. Chem. Rev.* **1999**, *190*−*192*, 1023. (b) Hashimoto, K.; Ohkoshi, S. *Philos. Trans. R. Soc. London, Ser. A* **1999**, *357*, 2977. (c) Mallah, T.; Marvilliers, A.; Rivière, E. *Philos. Trans. R. Soc. London, Ser. A* **1999**, *357*, 3139. (d) Miller, J. S. *MRS Bull.* **2000**, *25*, 60. (e) Verdaguer, M.; Galvez, N.; Garde, R.; Desplanches, C. *Electrochem. Soc. Interface* **2002**, *11*, 28. (f) Ohkoshi, S.; Hashimoto, K. *Electrochem. Soc. Interface* **2002**, *11*, 34.

(2) (a) Mallah, T.; Thiébaut, S.; Verdaguer, M.; Veillet, P. *Science* **1993**, *262*, 1554. (b) Ferlay, S.; Mallah, T.; Ouahès, R.; Veillet, P.; Verdaguer, M. *Nature* **1995**, *378*, 701. (c) Holmes, S. M.; Girolami, G. S. *J. Am. Chem. Soc.* **1999**, *121*, 5593. (d) Hatlevik, Ø.; Buschmann, W. E.; Zhang, J.; Manson, J. L.; Miller, J. S. *Adv. Mater.* **1999**, *11*, 914. (e) Ohkoshi, S.; Mizuno, M.; Hung, G. J.; Hashimoto, K. *J. Phys. Chem. B* **2000**, *104*, 9365.

(3) (a) Ohkoshi, S.; Arai, K.; Sato, Y.; Hashimoto, K. *Nat. Mater.* **2004**, *3*, 857. (b) Ohkoshi, S.; Abe, Y.; Fujishima, A.; Hashimoto, K. *Phys. Rev. Lett.* **1999**, *82*, 1285.

(4) (a) Margadonna, S.; Prassides, K.; Fitch, A. N. *J. Am. Chem. Soc.* **2004**, *126*, 15390. (b) Margadonna, S.; Prassides, K.; Fitch, A. N. *Angew. Chem., Int. Ed.* **2004**, *43*, 6316. (c) Coronado, E.; Giménez-López, M. C.; Levchenko, G.; Romero, F. M.; García-Baonza, V.; Milner, A.; Paz-Pasternak, M. *J. Am. Chem.* Soc. **2005**, *127*, 4580. (d) Kaye, S. S.; Long, J. R. *J. Am. Chem. Soc.* **2005**, *127*, 6506. (e) Catala, L.; Gacoin, T.; Boilot, J.-P.; Rivière, E.; Paulsen, C.; Lhotel, E.; Mallah, T. *Adv. Mater.* **2003**, *15*, 826. (f) Kosaka, W.; Nomura, K.; Hashimoto, K.; Ohkoshi, S. *J. Am. Chem. Soc.* **2005**, *127*, 8590. (g) Nuida, T.; Matsuda, T.; Tokoro, H.; Sakurai, S.; Hashimoto, K.; Ohkoshi, S. *J. Am. Chem. Soc.* **2005**, *127*, 11604.

(5) (a) Ohkoshi, S.; Hashimoto, K. *J. Photochem. Photobiol. C* **2001**, *2*, 71. (b) Dei, A. *Angew. Chem., Int. Ed.* **2005**, *44*, 1160. (c) Sato, O.; Iyoda, T.; Fujishima, A.; Hashimoto, K. *Science* **1996**, *272*, 704. (d) Ohkoshi, S.; Yorozu, S.; Sato, O.; Iyoda, T.; Fujishima, A.; Hashimoto, K. *Appl. Phys. Lett.* **1997**, *70*, 1040. (e) Ohkoshi, S.; Einaga, Y.; Fujishima, A.; Hashimoto, K. *J. Electroanal. Chem.* **1999**, *473*, 245. (f) Pejakoviæ, D. A.; Manson, J. L.; Miller, J. S.; Epstein, A. J. *Phys. Rev. Lett.* **2000**, *85*, 1994. (g) Varret, F.; Goujon, A.; Boukheddaden, K.; Noguès, M.; Bleuzen, A.; Verdaguer, M. *Mol. Cryst. Liq. Cryst.* **2002**, *379*, 333. (h) Tokoro, H.; Ohkoshi, S.; Hashimoto, K. *Appl. Phys. Lett.* **2003**, *82*, 1245. (i) Arimoto, Y.; Ohkoshi, S.; Zhong, Z. J.; Seino, H.; Mizobe, Y.; Hashimoto, K. *J. Am. Chem. Soc.* **2003**, *125*, 9240. (j) Gawali-Salunke, S.; Varret, F.; Maurin, I.; Enachescu, C.; Malarova, M.; Boukheddaden, K.; Codjovi, E.; Tokoro, H.; Ohkoshi, S.; Hashimoto, K. *J. Phys. Chem. B* **2005**, *109*, 8251.

 10.1021/ja0559092 CCC: $33.50

spin clusters from the assembly of octacyanometalates $[M(CN)_8]^{3-}$ ($M = Mo^V$, W^V) were prepared. Octacyanometalates $[M(CN)_8]^{n-}$ (M = Mo, W, etc.) are a versatile class of building blocks that adopt some different spatial configurations depending on their chemical environment, such as the surrounding ligands.[7] Thus, a variety of coordination geometries are found in the crystal structure of their complexes, i.e., zero-dimensional (0-D), 1-D, 2-D, and 3-D.[8] One attractive issue in the field of molecule-based magnets is the development of novel opto-functionalities.[5,9] In cyanometalate-based magnets, photoinduced magnetization was first observed in cobalt hexacyanoferrate,[5c,f,g,10] in which the electron transfer proceeds from Fe^{II} to Co^{III} by irradiation with visible light. Successively, photoinduced magnetic pole inversion was observed in a ferro/ferrimagnet composed of iron−manganese hexacyanochromate,[5d,11] which is caused by the optical control of the compensation temperature.[12,13,14]

One possible method for achieving optical control of spontaneous magnetization is to change the electron spin state of a magnetic material. For example, when irradiation varies the oxidation numbers of transition metal ions in a magnetic material, its magnetization changes. From this viewpoint, mixed-valence compounds[15] are considered to be suitable systems for observing photomagnetic phenomena. Mixed-valence compounds are usually divided into three categories: class I, class II, and class III, according to the magnitude of the mixed valency.[15c] Photoinduced electron transfer is often observed in class II compounds. Hennig et al. reported that $[Mo^{IV}(CN)_8]^{4-}$ and Cu^{2+} ions form a mixed-valence compound in aqueous solution, which exhibits an IT band around 500 nm.[16,17] The excitation of this band causes electron transfer to proceed from Mo^{IV} to Cu^{II} ions and produces a valence isomer, $Cu^I/[Mo^V(CN)_8]^{3-}$.[16c,18] When such a photoinduced electron transfer occurs in the corresponding solid compound, irradiation will change the magnetic properties; i.e., there is the possibility that the unpaired electrons of the produced Mo^V ($S = {}^1/_2$) and Cu^{II} ($S = {}^1/_2$) ions interact, leading to the ordering of the spins. Along this scenario, we investigated the photoinduced magnetic effect on a $Cu^{II}_2[Mo^{IV}(CN)_8]\cdot 8H_2O$ (**1**) solid and showed the preliminary results of this approach.[19] In this paper, we complete the study of **1** by reporting (i) the crystal structure of **1** by wide-angle X-ray scattering and X-ray absorption spectroscopies, (ii) the photomagnetic data of photoinduced magnetization, photoinduced exchange coupled system, photoreversibility, and thermal reversibility, (iii) the photoinduced change in the infrared (IR) spectra and UV−vis absorption spectra, and (iv) the mechanism of the photomagnetism.

2. Experimental Section

2.1. Synthesis and Physical Characterization. The target compound was prepared by reacting an aqueous solution of $K_4[Mo(CN)_8]\cdot 2H_2O$ (0.2 mol dm^{-3}) with an aqueous solution of $CuCl_2\cdot 2H_2O$ (0.2 mol dm^{-3}). The precipitated product was filtered, washed with H_2O, and air-dried. To measure accurate UV−vis absorption spectra, a film-type of the target compound was also prepared on a SnO_2-coated glass by an electrochemical method (Supporting Information).

Elemental analyses were conducted by inductively coupled plasma mass spectroscopy (ICP-MS) and standard microanalysis methods. The UV−visible absorption spectra were measured by a Shimadzu UV-3100 spectrometer. The IR spectra were recorded on a Shimadzu FT-IR 8200PC spectrometer. The X-ray powder diffraction (XRD) patterns were measured by a Rigaku RINT2100 spectrometer. Magnetic susceptibility and magnetization measurements were conducted using a Quantum Design MPMS superconducting quantum interference device (SQUID) magnetometer.

2.2. Wide-Angle X-ray Scattering. Powder of **1** was sealed in a Lindemann capillary. The scattering diffusion spectrum of the samples irradiated with graphite-monochromatized Mo Kα radiation (λ =

(6) (a) Larionova, J.; Clérac, R.; Sanchiz, J.; Kahn, O.; Golhen, S.; Ouahab, L. *J. Am. Chem. Soc.* **1998**, *120*, 13088. (b) Larionova, J.; Kahn, O.; Gohlen, S.; Ouahab, L.; Clérac, R. *J. Am. Chem. Soc.* **1999**, *121*, 3349.
(7) Leipoldt, J. G.; Basson, S. S.; Roodt, A. *Adv. Inorg. Chem.* **1993**, *40*, 241.
(8) (a) Zhong, Z. J.; Seino, H.; Mizobe, Y.; Hidai, M.; Fujishima, A.; Ohkoshi, S.; Hashimoto, K. *J. Am. Chem.* Soc. **2000**, *122*, 2952. (b) Larionova, J.; Gross, M.; Pilkington, M.; Andres, H.; Stoeckli-Evans, H.; Güdel, H. U.; Decurtins, S. *Angew. Chem., Int. Ed.* **2000**, *39*, 1605. (c) Sieklucka, B.; Szklarzewicz, J.; Kemp, T. J.; Errington, W. *Inorg. Chem.* **2000**, *39*, 5156. (d) Podgajny, R.; Desplanches, C.; Sieklucka, B.; Sessoli, R.; Villar, V.; Paulsen, C.; Wernsdorfer, W.; Dromzee, Y.; Verdaguer, M. *Inorg. Chem.* **2002**, *41*, 1323. (e) Rombaut, G.; Golhen, S.; Ouahab, L.; Mathonière, C.; Kahn, O. *J. Chem. Soc., Dalton Trans.* **2000**, 3609. (f) Li, D. F.; Gao, S.; Zheng, L. M.; Tang, W. X. *J. Chem. Soc., Dalton Trans.* **2002**, 2805. (g) Podgajny, R.; Korzeniak, T.; Balanda, M.; Wasiutynski, T.; Errington, W.; Kemp, T. J.; Alcock, N. W.; Sieklucka, B. *Chem. Commun.* **2002**, 1138. (h) Ohkoshi, S.; Arimoto, Y.; Hozumi, T.; Seino, H.; Mizobe, Y.; Hashimoto, K. *Chem. Commun.* **2003**, 2772. (i) Garde, R.; Desplanches, C.; Bleuzen, A.; Veillet, P.; Verdaguer, M. *Mol. Cryst. Liq. Cryst.* **1999**, *334*, 587. (j) Zhong, Z. J.; Seino, H.; Mizobe, Y.; Hidai, M.; Verdaguer, M.; Ohkoshi, S.; Hashimoto, K. *Inorg. Chem.* **2000**, *39*, 5095. (k) Meske, W.; Babel, D. *Z. Anorg. Allg. Chem.* **1999**, *625*, 51. (l) Li, D. F.; Gao, S.; Zheng, L. M.; Sun, W. Y.; Okamura, T.; Ueyama, N.; Tang, W. X. *New J. Chem.* **2002**, *26*, 485. (m) Sra, A. K.; Rombaut, G.; Lahitete, F.; Golhen, S.; Ouahab, L.; Mathonière, C.; Yakhmi, J. V.; Kahn, O. *New J. Chem.* **2000**, *24*, 871. (n) Korzeniak, T.; Stadnicka, K.; Rams, M.; Sieklucka, B. *Inorg. Chem.* **2004**, *43*, 4811. (o) Korzeniak, T.; Stadnicka, K.; Pelka, R.; Balanda, M.; Tomala, K.; Kowalski, K.; Sieklucka, B. *Chem. Commun.* **2005**, 2939. (p) Hozumi, T.; Ohkoshi, S.; Arimoto, Y.; Seino, H.; Mizobe, Y.; Hashimoto, K. *J. Phys. Chem. B* **2003**, *107*, 11571. (q) Song, Y.; Ohkoshi, S.; Arimoto, Y.; Seino, H.; Mizobe, Y.; Hashimoto, K. *Inorg. Chem.* **2003**, *42*, 1848. (r) Withers, J. R.; Ruschmann, C.; Bojang, P.; Parkin, S.; Holmes, S. M. *Inorg. Chem.* **2005**, *44*, 352.
(9) (a) Gütlich, P.; Garcia, Y.; Woike, T. *Coord. Chem. Rev.* **2001**, *219*, 839. (b) Gütlich, P.; Hauser, A.; Spiering, H. *Angew. Chem., Int. Ed. Engl.* **1994**, *33*, 2024. (c) Létard, J. F.; Real, J. A.; Moliner, N.; Gaspar, A. B.; Capes, L.; Cador, O.; Kahn, O. *J. Am. Chem. Soc.* **1999**, *121*, 10630. (d) Létard, J. F.; Guionneau, P.; Codjovi, E.; Lavastre, O.; Bravic, G.; Chasseau, D.; Kahn, O. *J. Am. Chem. Soc.* **1997**, *119*, 10861. (e) Boukheddaden, K.; Shteto, I.; Hôo, B.; Varret, F. *Phys. Rev. B* **2000**, *62*, 14806. (f) Ogawa, Y.; Koshihara, S.; Koshino, K.; Ogawa, T.; Urano, C.; Takagi, H. *Phys. Rev. Lett.* **2002**, *84*, 3181. (g) Renz, F.; Oshio, H.; Ksenofontov, V.; Waldeck, M.; Spiering, H.; Gütlich, P. *Angew. Chem., Int. Ed.* **2000**, *39*, 3699.
(10) (a) Sato, O.; Einaga, Y.; Iyoda, T.; Fujishima, A.; Hashimoto, K. *J. Electrochem. Soc.* **1997**, *144*, 11. (b) Shimamoto, N.; Ohkoshi, S.; Sato, O.; Hashimoto, K. *Inorg. Chem.* **2002**, *41*, 678. (c) Bleuzen, A.; Lomenech, C.; Escax, V.; Villain, F.; Varret, F.; Cartier dit Moulin, C.; Verdaguer, M. *J. Am. Chem. Soc.* **2000**, *122*, 6648. (d) Cartier dit Moulin, C.; Villain, F.; Bleuzen, A.; Arrio, M. A.; Sainctavit, P.; Lomenech, C.; Escax, V.; Baudelet, F.; Dartyge, E.; Gallet, J. J.; Verdaguer, M. *J. Am. Chem. Soc.* **2000**, *122*, 6653.
(11) Ohkoshi, S.; Hashimoto, K. *J. Am. Chem. Soc.* **1999**, *121*, 10591.
(12) Ohkoshi, S.; Iyoda, T.; Fujishima, A.; Hashimoto, K. *Phys. Rev. B* **1997**, *56*, 11642.
(13) Néel, L. *Ann. Phys.* **1948**, *3*, 137.
(14) (a) Mathonière, C.; Carling, S. G.; Yusheng, D.; Day, P. *J. Chem. Soc., Chem. Commun.* **1994**, 1551. (b) Mathonière, C.; Nuttall, C. J.; Carling, S. G.; Day, P. *Inorg. Chem.* **1996**, *35*, 1201.
(15) (a) Brown, D. B. *Mixed Valence Compounds*; NATO ASI; Reidel: Dordrecht, 1980. (b) Prassides, K. *Mixed Valency Systems: Applications in Chemistry, Physics and Biology*; NATO ASI; Kluwer: Dordrecht, 1991. (c) Robin, M. B.; Day, P. *Adv. Inorg. Chem. Radiochem.* **1967**, *10*, 247. (d) Hush, N. S. *Prog. Inorg. Chem.* **1967**, *8*, 391. (e) Piepho, S. B.; Krausz, E. R.; Schatz, P. N. *J. Am. Chem. Soc.* **1978**, *100*, 2996. (f) Bernhardt, P. V.; Bozoglián, F.; Macpherson, B. P.; Martínez, M. *Coord. Chem. Rev.* **2005**, *249*, 1902. (g) Berlinguette, C. P.; Dragulescu-Andrasi, A.; Sieber, A.; Güdel, H. U.; Achim, C.; Dunbar, K. R. *J. Am. Chem. Soc.* **2005**, *127*, 6766.
(16) (a) Hennig, H.; Rehorek, A.; Rehorek, D.; Thomas, P. *Inorg. Chim. Acta* **1984**, *86*, 41. (b) Rehorek, D.; Salvetter, J.; Hantschmann, A.; Hennig, H.; Stasicka, Z.; Chodkowska, A. *Inorg. Chim. Acta* **1979**, *37*, L471. (c) Hennig, H.; Rehorek, A.; Rehorek, D.; Thomas, P. *Inorg. Chim. Acta* **1983**, *77*, L11.
(17) Sieklucka, B. *Prog. React. Kinet.* **1989**, *15*, 175.
(18) Since this system is a Lewis acid−base adduct which undergoes photoinduced electron transfer, it can be also called the valence tautomeric system.
(19) (a) Ohkoshi, S.; Machida, N.; Zhong, Z. J.; Hashimoto, K. *Synth. Met.* **2001**, *122*, 523. (b) Rombaut, G.; Verelst, M.; Golhen, S.; Ouahab, L.; Mathonière, C.; Kahn, O. *Inorg. Chem.* **2001**, *40*, 1151. (c) Ohkoshi, S.; Machida, N.; Abe, Y.; Zhong, Z. J.; Hashimoto, K. *Chem. Lett.* **2001**, 312.

0.71069 Å) was obtained using a LASIP diffractometer.[20] A total of 457 intensities corresponding to equidistant points ($s = 4\pi(\sin\theta/\lambda)$; $\Delta s = 0.035$ Å^{-1}) were collected in the range $0 < \theta < 65°$. Immediately afterward, measurements of air and Lindemann capillary diffusion were done under exactly the same conditions. The scattered intensity (sample + air + capillary) of the raw sample was corrected for air and capillary contributions by spectral subtraction, taking into account absorption from the sample, and then corrected for polarization and self-absorption effects. Normalization was performed using the method of Norman and Krogh-Moe.[21] The atomic scattering factors were taken from Cromer and Waber.[22] The reduced experimental radial distribution function (RDF) was calculated by a procedure similar to that given in ref 23. The theoretical RDF was computed from the structural models by Fourier transform of the theoretical intensities calculated using Debye's formula.[24]

2.3. X-ray Absorption Spectroscopy (XAS) Recording and Analysis. XAS experiments were performed at LURE, the French synchrotron facility, on the XAS 13 beam line. At the Cu K-edge, X-ray absorption near-edge structure (XANES) spectra were recorded with a Si 311 double-crystal monochromator. Energy calibration was performed with a Cu metal foil for which the first inflection point of the absorption K-edge was set at 8979 eV. Extended X-ray absorption fine structure (EXAFS) spectra were recorded with a Si 111 "channel-cut" monochromator. The experiments were carried out in transmission mode on samples prepared in the form of thin self-supporting wafers. After removal of the background, the XANES spectra were normalized at the middle of the first EXAFS oscillation to allow comparison. The two first steps of the EXAFS signal treatment were performed with the "EXAFS pour le Mac" code.[25] The EXAFS signal was extracted from the data by subtracting a linear pre-edge background and a combination of polynomials and cubic spline atomic absorption background and was normalized by the Lengeler−Eisenberger procedure.[26] The pseudoradial distribution functions are given by the Fourier fransform (FT) of $w(k)k^3\chi(k)$, where $w(k)$ is a Kaissel−Bessel window with a smoothness parameter equal to 3 (k is the wavenumber). The k range is limited to 3.0−14.0 Å^{-1} ($\Delta k = 11$ Å^{-1}). Due to the multiple scattering events expected in compounds with such geometry, the EXAFS simulation in the framework of single scattering is only possible for the first shell of neighbors. Therefore, we used the FEFF7 code with multiple scattering for the quantitative analysis of the following shells.[27]

2.4. Photomagnetic Effect. The experimental conditions of the light irradiation measurements in SQUID were as follows: for the measurements of magnetization vs temperature and magnetization vs external magnetic field curves, the continuous-wave (CW) Kr^+ laser with wavelength (λ) of 413 nm and diode lasers with $\lambda = 473$, 658, 785, and 840 nm were used as light sources. The sample, spread on an adhesive tape, was placed on the edge of an optical fiber in SQUID. The measurements for wavelength dependence of excitation in the change of magnetization were carried out using the OPO laser (430−650 nm) pumped by a Nd:YAG laser (repetition = 10 Hz, pulse width = 6 ns). The light irradiation measurement in IR spectroscopy was carried out using 473-nm diode laser light. The light irradiation measurement in UV−vis absorption spectroscopy was carried out using 473-, 658-, 785-, and 840-nm diode laser lights.

3. Results and Discussion

3.1. Material and Structure. The prepared compound **1** is a violet powder. Elemental analyses of the prepared sample showed that the formula for **1** is $Cu^{II}_2[Mo^{IV}(CN)_8]\cdot 8H_2O$. Calcd: Cu, 22.09; Mo, 16.68; C, 16.70; N, 19.48; H, 2.80. Found: Cu, 22.10; Mo, 16.32; C, 16.33; N, 19.50; H, 2.85. The CN stretching frequency for **1** was observed at 2162 cm^{-1} in the IR spectra. The UV−vis spectrum showed the intervalence-transfer (IT) band between $Mo^{IV}-CN-Cu^{II}$ and $Mo^{V}-CN-Cu^{I}$ around 480 nm, which almost corresponded to the optical absorption spectra in the solution of $Cu^{II}/[Mo^{IV}(CN)_8]$.[16a,b]

The X-ray powder diffraction pattern of **1** shows some large peaks, indicating that **1** is poorly crystalline (Supporting Information). The crystal structures of analogues with the formula of $M^{II}_2[Mo^{IV}(CN)_8]\cdot zH_2O$, where M = Mn(II), Fe(II), or Co(II),[8m,28,29] were solved in the tetragonal system *I*4/*m*. These analogues have a 3D architecture within a highly symmetrical alternation of $Mo(CN)_8$ and $M(H_2O)_2$ units, and the cyano groups act as bridges. To obtain structural information about **1**, wide-angle X-ray scattering (WAXS) and X-ray absorption spectroscopies (XANES and EXAFS) studies were performed for **1** and compared to the structural data for the analogues.

The WAXS technique is useful since it provides information about the connectivity in a polymeric material. The WAXS spectra are given in the Supporting Information. The comparison of the Fe and Mn analogues is consistent with their isostructurality, and the small observed differences are due to the different sizes of the 3d ions. For the three compounds, down to 6 Å, the similarities of the RDFs indicate analogous Mo−CN−M cores. The Mo···Cu distance is 5.25 Å, which is shorter than the Mo···Fe distance (5.40 Å) in the Fe analogue, or the Mo···Mn distance (5.48 Å) in the Mn analogue, consistent with the smaller ionic radius of the Cu^{2+} compared to the Fe^{2+} and Mn^{2+}. However, the RDFs show important differences in the 6−10 Å area, which mainly represents the M···M distances. The Mo···Mo distances are 10.15 Å for **1**, 10.60 Å for the Fe analogue, and 10.80 Å for the Mn analogue.

The XANES and EXAFS studies are crucial for understanding the local environment around the metallic centers.[30] EXAFS determines the distances between the absorber and the neighboring first shells. The XANES part of the spectrum is sensitive to the electronic structure of the absorber (oxidation and spin state, local symmetry, etc.). XANES was recorded for **1** at the Cu K-edge. By comparison to the XANES spectra of the model compounds, XANES can be used as fingerprint for the local symmetry of the Cu^{II} ions. Figure 1 compares the XANES of **1** with the spectra of copper model compounds in various geometries. For $Cu(en)_2$ (en = ethylenediamine), peak A is the signature of the square planar geometry[31] and is not observed in the spectra of the other compounds, $Cu(en)_3$ (distorted

(20) The LASIP diffractometer has a geometry especially designed for scattering measurements since it minimizes every external parasitic scattering phenomenon.
(21) (a) Norman, N. *Acta Crystallogr.* **1957**, *10*, 370. (b) Krogh-Moe, J. *Acta Crystallogr.* **1956**, *9*, 951.
(22) Cromer, D.; Waber, T. *International Tables for X-ray Crystallography*; Kynoch Press: Birmingham, 1974; Vol. 4.
(23) (a) Mosset, A.; Lecante, P.; Galy, J. *Philos. Mag. B* **1982**, *46*, 137. (b) Burian, A.; Lecante, P.; Mosset, A.; Galy, J. *J. Non-Cryst. Solids* **1987**, *90*, 633. (c) Laberty, C.; Verelst, M.; Lecante, P.; Alphonse, P.; Mosset, A.; Rousset, A. *J. Solid State Chem.* **1997**, *129*, 271. (d) Verelst, M.; Sommier, L.; Lecante, P.; Mosset, A.; Kahn, O. *Chem. Mater.* **1998**, *10*, 980. (e) Cador, O.; Mathonière, C.; Kahn, O.; Costes, J.-P.; Verelst, M.; Lecante, P. *Inorg. Chem.* **1999**, *38*, 2643.
(24) Debye, P. *Ann. Phys. (Leipzig)* **1915**, *46*, 809.
(25) Michalowicz, A. *EXAFS pour le MAC*; Société Française de Chimie: Paris, 1991.
(26) Lengeler, B.; Eisenberger, P. *Phys. Rev. B* **1980**, *21*, 4507.
(27) Rehr, J. J.; Mustre de Leon, J.; Zabinsky, S. I.; Albers, R. C. *J. Am. Chem. Soc.* **1991**, *113*, 5135.
(28) Willemin, S.; Larionova, J.; Clérac, R.; Donnadieu, B.; Henner, B.; Le Goff, X. F.; Guérin, C. *Eur. J. Inorg. Chem.* **2003**, 1866.
(29) Tuna, F.; Golhen, S.; Ouahab, L.; Sutter, J.-P. *C. R. Chimie* **2003**, *6*, 377.
(30) Teo, B. *EXAFS: Basic Principles and Data Analysis, Inorganic Chemistry Concepts*; Springer-Verlag: Berlin, 1986; Vol. 9.

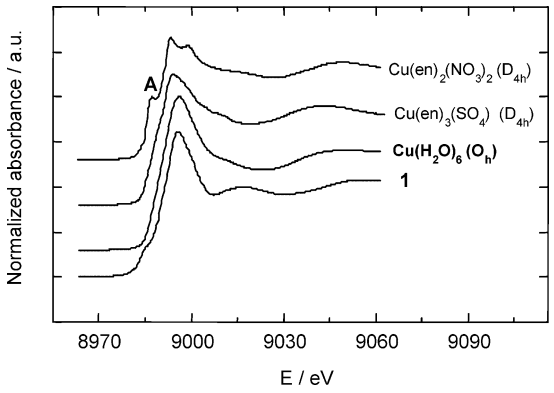

Figure 1. XANES K-edge spectra for $Cu(en)_2(NO_3)_2$ (D_{4h} square planar), $Cu(en)_3(SO_4)$ (D_{4h}), $Cu(H_2O)_6$ in solution (close to O_h), and **1**.

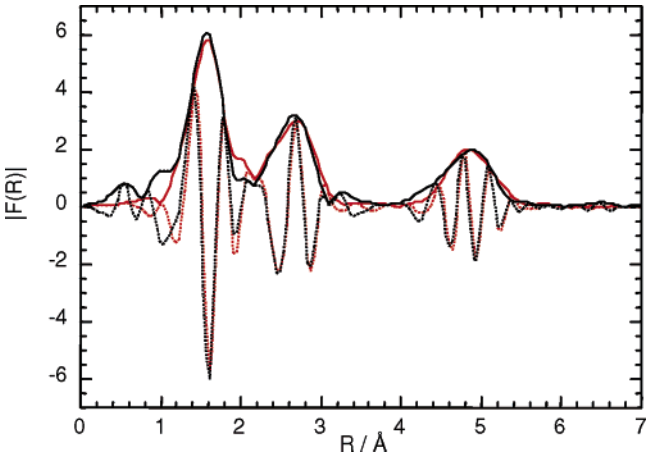

Figure 2. EXAFS Fourier transform module (experimental spectrum, black solid line; calculated spectrum, red solid line) and imaginary part (experimental spectrum, black dotted line; calculated spectrum, red dotted line) at Cu K-edge for **1**.

octahedron, four short distances at 2.04 Å and two long at 2.23 Å) and $Cu(H_2O)_6$ (quite octahedral with six distances close to 1.99 Å).[32]

Peak A is also absent in the XANES of **1**, which unambiguously excludes the square planar symmetry for copper. The spectrum of **1** is slightly different from that of $Cu(en)_3$ but is quite similar to the XANES of $Cu(H_2O)_6$, except for the shoulder at the beginning of the edge jump always observed in compounds with CN ligands. Therefore, we propose that the copper ions have a quite octahedral symmetry with a dispersion of Cu−N,O distances always observed when the Jahn−Teller effect is expected. The Fourier transform of the experimental EXAFS signal (Figure 2) displays three peaks assigned to the three first shells around the copper. The first peak of the Fourier transform corresponds to two subshells: nitrogen neighbors (Cu−N, from cyanide) and oxygen ones (Cu−O, from linked water). The second peak corresponds to the carbon atom of the cyanide ligands, and the third one corresponds to the molybdenum atoms. EXAFS quantitative analysis of the first coordination shell confirms the XANES conclusion. The best simulation is obtained for six neighbors at 1.98 Å with an important Debye−Waller factor (σ = 0.09 Å compared to the 0.05 Å value generally found for regular octahedra), which traduces an important radial distribution of the distances around 1.98 Å due to the Jahn−Teller distortion.

This distance is close to the Cu−O distance in $Cu(H_2O)_6$ (1.99 Å). Analysis of the complete EXAFS signal was performed with the FEFF code in order to account for multiple scattering events. The best agreement between the Fourier transform of the experimental EXAFS spectrum and the calculated one (Figure 2) has been obtained following a procedure similar to the one previously described.[33] We found the following structural parameters: six first O,N neighbors at 1.98 Å, distance given by the EXAFS first shell analysis; d(C−N) = 1.16 Å, typical distance for a cyanide ligand; and d(Mo−C) = 2.16 Å, distance from the XRD measurements in the analogues. The Cu−N−C angle is equal to 165°, with a linear expected Mo−C−N geometry and a distance Mo···Cu equal to 5.26 Å. The quantitative analysis of the EXAFS spectrum recorded at the Mo K-edge, not presented here, gives the same structural parameters. These results are consistent with the Mo···Cu distances found by WAXS, given the precision of these two techniques. In conclusion, we have shown that **1** is an extended network with the following structural features: (i) the shortest Mo···Mo distance in the polymeric network is 10.15 Å, (ii) the geometry for the copper ions with six Cu−(N,O) neighbors at 1.98 Å is quite octahedral, and (iii) the structural arrangement of the metallic cores in the network of **1** generates bent Cu−N−C−Mo entities.

3.2. Photomagnetism. 3.2.1. Photoinduced Magnetization and Light-Reversibility. The SQUID measurement indicates that before irradiation, **1** is paramagnetic due to Cu^{II}. Irradiating **1** with a blue CW diode laser light (473 nm, 35 mW cm^{-2}) at 3 K gradually increases the magnetization at H = 20 G, as shown in Figure 3a. After irradiation for 30 min (A), the irradiated sample exhibits a spontaneous magnetization with a Curie temperature (T_C) of 13 K (Figure 3b, black closed circles). When the sample is warmed above 250 K and cooled to 3 K, the magnetic property returns to the initial state. After that, when the sample is irradiated for 165 min (B), the magnetization further increases and the irradiated sample exhibits a T_C of 25 K (Figure 3b, red closed circles). The magnetization vs external magnetic field plots show that the magnetization value is 1.8 μ_B and the coercive field (H_c) is 34 G at 3 K when the sample is irradiated for 165 min (Supporting Information).

To study the photoreversibility, the wavelength dependence on the excitation was investigated using pulsed-laser light in the visible region. Figure 4 shows the wavelength of the excitation vs the change in magnetization by irradiation with visible pulsed-laser lights. When **1** is irradiated with laser light below 520 nm, the magnetization increases. Conversely, irradiating with laser light above 520 nm decreases the produced magnetization, demonstrating visible-light reversibility. Figure 5a shows the magnetization vs temperature plots during irradiation with 473-, 658-, 785-, and 840-nm CW diode lasers. Irradiating with the 473-nm laser light (35 mW cm^{-2}) for 165 min at 3 K causes a spontaneous magnetization with a T_C of 25 K (Figure 5a, closed circles). When this sample is subsequently irradiated with 658-nm laser light (20 mW cm^{-2}), the magnetization values decrease, but the change in the magnetization plateaus (Figure 5b). Successively, when the sample is irradiated

(31) Cartier dit Moulin, C.; Momenteau, M.; Dartyge, E.; Fontaine, A.; Tourillon, G.; Michalowicz, A.; Verdaguer, M. *J. Chem. Soc., Dalton Trans.* **1992**, 609.
(32) (a) Villain, F. Ph.D. Thesis, Paris 6 University, 1998. (b) Villain, F.; Verdaguer, M.; Dromzee, M. *J. Phys. IV* **1997**, *7*, 659.
(33) Garde, R.; Villain, F.; Verdaguer, M. *J. Am. Chem. Soc.* **2002**, *124*, 10531.

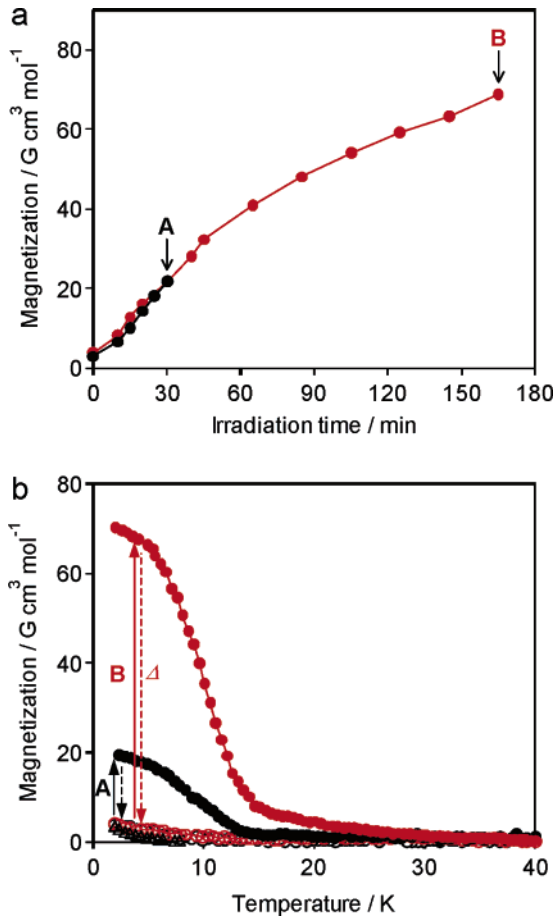

Figure 3. (a) Magnetization vs irradiation time curves for **1** at 3 K in a 20 G external magnetic field (light irradiation, 473 nm, 35 mW cm^{-2}). Experimental sequence: light irradiation for 30 min at 3 K (black closed circle) (**A**) → 250 K (thermal treatment) → 3 K → light irradiation for 165 min (red closed circle) (**B**). (b) Magnetization vs temperature curves of **1** in a 20 G external magnetic field upon irradiation with light (473 nm, 35 mW cm^{-2}). Magnetic measurement sequence: 40 K → (black open circle) → 3 K (light irradiation for 30 min) (**A**) → 40 K→ (black closed circle) → 3 K → 250 K (thermal treatment) → 40 K → (black open triangle) → 3 K (light irradiation for 165 min) (**B**) → 40 K → (red closed circle) → 3 K → 250 K (thermal treatment) → 40 K → (red open circle) → 3 K.

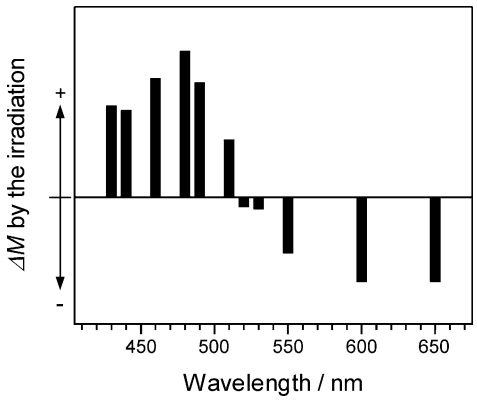

Figure 4. Wavelength of the excitation pulsed laser vs the change in magnetization (ΔM).

with 785-nm laser light (45 mW cm^{-2}), the magnetization decreases. Furthermore, the spontaneous magnetization completely disappears after irradiation with 840-nm light (60 mW cm^{-2}). This equilibrium behavior suggests that a photostationary

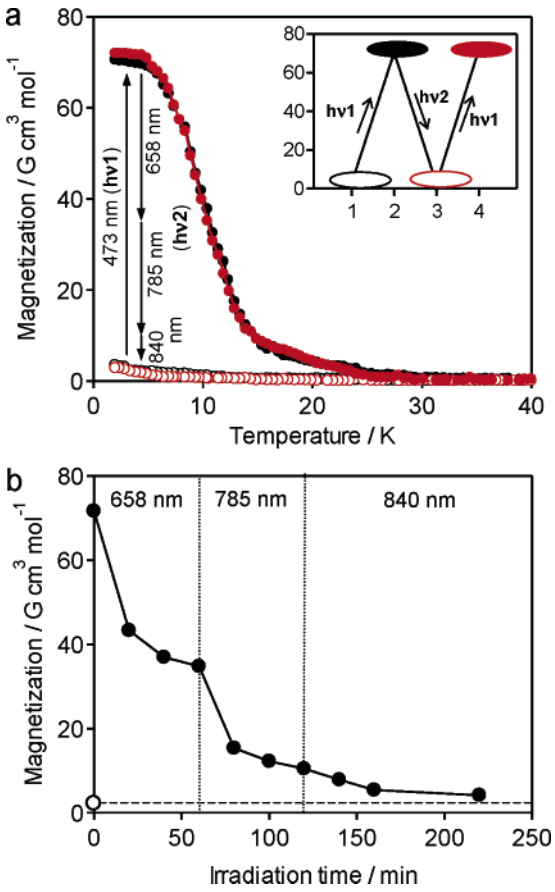

Figure 5. Light-induced reversible magnetization in **1** under a 20 G external magnetic field at 3 K. (a) Magnetization vs temperature curves before and after irradiation. Measurement sequence: 40 K → (black open circle) → 3 K (light irradiation with 473-nm light of 35 mW cm^{-2}) → 40 K → (black closed circle) → 3 K (light irradiation with 658-, 785-, and 840-nm lights of 20, 45, and 60 mW cm^{-2}, respectively) → 40 K → (red open circle) → 3 K (light irradiation with 473 nm of 35 mW cm^{-2}) → 40 K → (red closed circle) → 3 K. (Inset) Magnetization change caused by irradiation with 473-nm light ($h\nu_1$) (black closed circle), 658-, 785-, and 840-nm lights ($h\nu_2$) (red open circle), and 473-nm light ($h\nu_1$) (red closed circle). (b) Magnetization vs irradiation time curve of the photoreverse process in a 20 G external magnetic field upon irradiation with light (658-, 785-, and 840-nm lights of 20, 45, and 60 mW cm^{-2}, respectively). The open circle on the vertical axis is the initial magnetization value.

state between the photoreduced magnetization and the photoinduced magnetization is established. The present photoreversibility of the magnetization in **1** can be repeated, as shown in the inset of Figure 5a.

3.2.2. Photoinduced Exchange-Coupled System and Thermal Reversibility. As mentioned in section 3.2.1, the return to the initial state occurs in the paramagnetic region below 250 K. When **1** is irradiated with a weak light intensity (413 nm, 3 mW cm^{-2}, 6 h), **1** is converted into an *exchange-coupled system*. Saturation in the magnetic susceptibility is not observed, and the product of molar magnetic susceptibility and temperature ($\chi_M T$) vs T curve has physical meaning. Figure 6a shows the $\chi_M T$ vs T curves for **1** before and after irradiation in the warming mode (0.3 K min^{-1}, $H = 5000$ G) and after a room-temperature treatment. Before irradiation, the curve is typical of a paramagnetic system with two spins of $S = {}^1/_2$ and weak antiferromagnetic interactions that appear below 20 K. The experimental value is 0.79 cm^3 mol^{-1} K, which is consistent with the Curie value, 0.75 cm^3 mol^{-1} K, assuming $g = 2$. After irradiation,

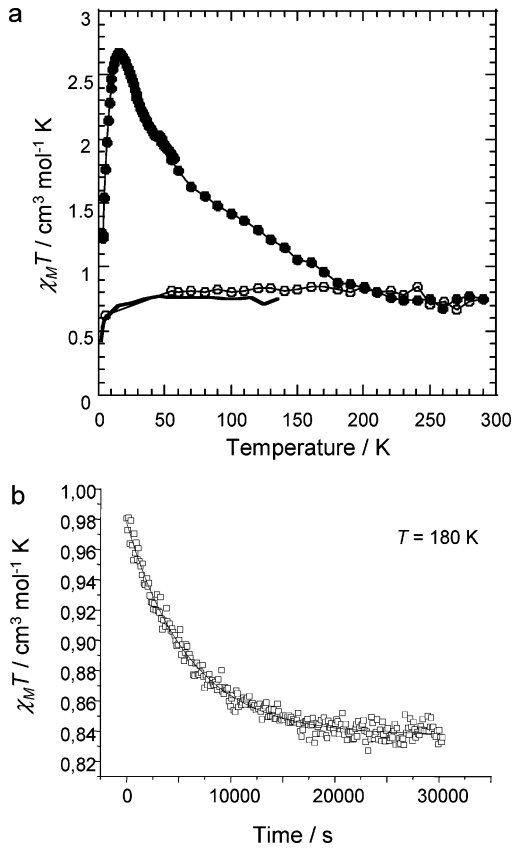

Figure 6. (a) $\chi_M T$ vs T before (○) and after (●) blue light irradiation at 10 K for **1** under a 5000 G field and (—) after heating to 300 K. (b) Time relaxation of $\chi_M T$ at 180 K.

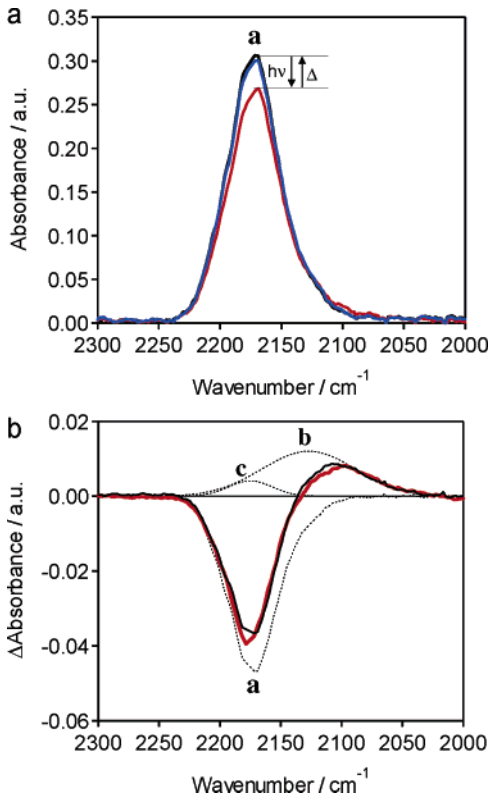

Figure 7. (a) IR spectra at 3 K before irradiation with light (black line), after irradiation with light (red line), and after a thermal treatment of 250 K (blue line). (b) The differential spectra (red line) and waveform separation (black dotted lines). The black solid line is a total curve of peaks of **a**, **b**, and **c**.

$\chi_M T$ initially increases with T between 2 and 15 K and then decreases with temperature above 15 K. The maximum value of $\chi_M T$ is 2.7 cm^3 mol^{-1} K at 15 K. Finally, the two curves are superimposed for temperatures above 200 K. The $\chi_M T$ vs T curve obtained after a room-temperature treatment perfectly fits the $\chi_M T$ vs T curve in the initial state, illustrating the full reversibility of the process.

Kinetics studies were conducted at different temperatures: T = 5, 25, 50, 100, 160, and 180 K. These studies were performed using the following procedure: (i) irradiation at 10 K; (ii) the laser irradiation is stopped and the temperature is immediately increased to the desired temperature; (iii) when the temperature is stable, the study of $\chi_M T$ vs time is initiated; and (iv) if the signal decreases during step (iii), then a new population experiment is performed as indicated in step (i). The $\chi_M T$ value remains constant for several hours at T = 5, 25, and 50 K, which indicates that the magnetic signal in the low-temperature range is stable. For temperatures above 100 K, $\chi_M T$ decreases with time. After 4 h in the dark, the relaxation is incomplete at 100 and 160 K, which results in a net decrease of 2% between the initial value (1.54 cm^3 mol^{-1} K) and the final value (1.51 cm^3 mol^{-1} K) at 100 K and a net decrease of 11% between the initial value (1.05 cm^3 mol^{-1} K) and the final value (0.93 cm^3 mol^{-1} K) at 160 K. Figure 6b shows the time decay of $\chi_M T$ at 180 K. At this temperature, the relaxation is complete and the final value (0.84 cm^3 mol^{-1} K) is close to the $\chi_M T$ value before irradiation. The decrease may be fitted with a single-exponential decay, giving τ = 5900 s, which implies that the relaxation is slow.

The relaxation data show that below 100 K, the photoinduced magnetic signal is very stable. The $\chi_M T$ vs T plot is the result of the exchange interactions between the magnetic centers. The behavior in the 15−100 K range is due to ferromagnetic interactions that appears in the photoproduct **1′**. Below 15 K, the antiferromagnetic interactions cause $\chi_M T$ to decrease. The shape of the curve (T < 100 K) is close to the ones obtained for *high-spin* clusters except that additional antiferromagnetic intercluster interactions appear at very low temperature. The formation of these clusters would correspond to the formation of magnetic *dots* in the solid state, which would increase in size under light excitation. Above 100 K, the relaxation dynamics and magnetic interactions are superimposed. Above 200 K, the initial state is completely restored. Compared to other photomagnetic materials, **1** has a highly stable photoinduced state.

3.2.3. Photoinduced Change in IR Spectra and UV−Vis Absorption Spectra. The IR spectra after irradiation were measured to understand the mechanism of the photomagnetic behaviors. Figure 7a shows the IR spectra after irradiation with 473-nm light (35 mW cm^{-2}) for 30 min at 3 K, which decreases the IR peak due to Mo^{IV}−CN−Cu^{II} at 2170 cm^{-1} (peak a).[34] Figure 7b shows the difference in the spectra before and after irradiation. This differential spectrum can be fitted by combining three peaks: the negative peak **a** and two positive new peaks, **b** (2127 cm^{-1}) and **c** (2175 cm^{-1}). The formula of the sample during irradiation is expressed as $Cu^{II}_{2-x}Cu^{I}_{x}[Mo^{IV}(CN)_8]_{1-x}[Mo^{V}$-

(34) The volume contraction causes the CN stretching peak to gradually shift from 2162 cm^{-1} at room temperature to 2170 cm^{-1} at 3 K.

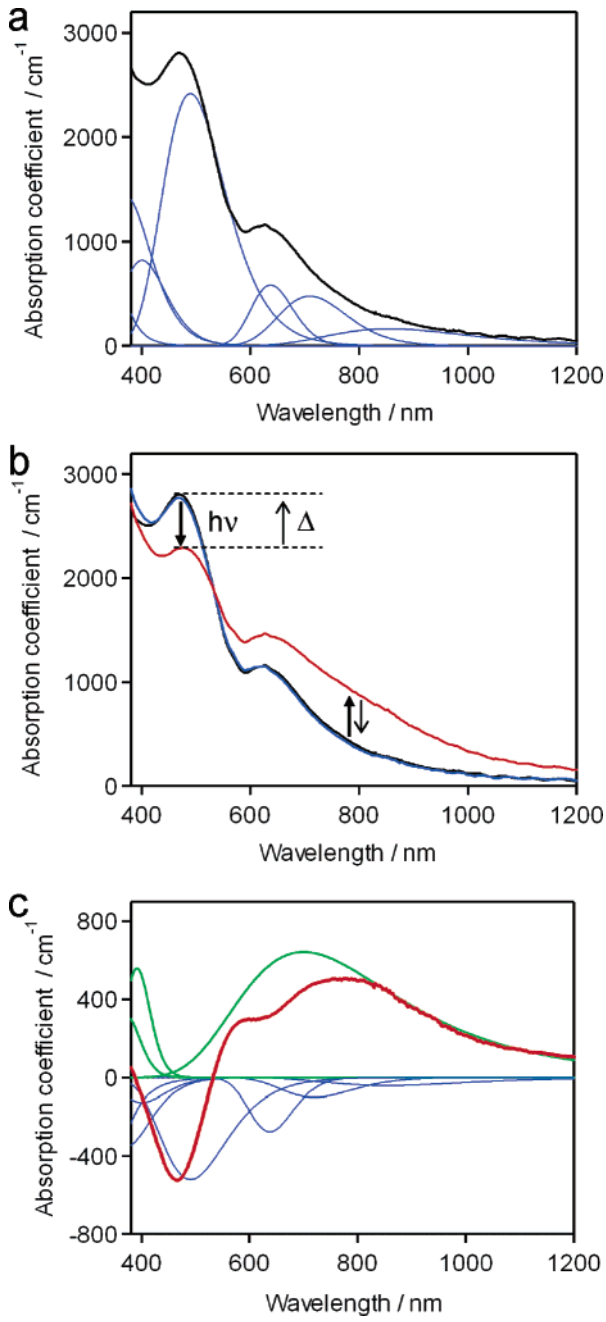

Figure 8. (a) UV−vis absorption spectra of a film-type of **1** before irradiation with light (black line) at 3 K and waveform separation (blue lines): MLCT band of $Mo^{IV} \rightarrow CN$ (250 nm), d−d transition of Mo^{IV} (370 and 400 nm), IT band (483 nm), and d−d transition of Cu^{II} (637, 719, and 855 nm). (b) UV−vis absorption spectra at 3 K before (black line) and after irradiation with 473-nm light (35 mW cm^{-2} for 60 min) (red line) and after thermal treatment above 250 K (blue line). (c) The differential spectrum of the spectra before and after irradiation with light (red line) and the waveform separation of the differential spectra. The blue lines are the same as above, and the green lines are induced by irradiation: LMCT bands of $CN \rightarrow Mo^{V}$ (370 and 390 nm) and *reverse*-IT band (710 nm).

$(CN)_8]_x \cdot 8H_2O$, which depends on the photoinduced electron-transfer ratio x ($0 \le x \le 1$) from Mo^{IV} to Cu^{II}. The probabilities of $Mo^{IV}-CN-Cu^{II}$, $Mo^{IV}-CN-Cu^{I}$, $Mo^{V}-CN-Cu^{II}$, and $Mo^{V}-CN-Cu^{I}$ existing are described by $(1-x)(2-x)/2$, $(1-x)x/2$, $x(2-x)/2$, and $x^2/2$, respectively. In addition, the oscillator strength of the CN bridged to Mo^{IV} is about 10 times larger than that of the CN bridged to Mo^{V}.[8] The intensity ratio of **a**:**b**:**c** in the present irradiated sample is 20:1:0.3, which is

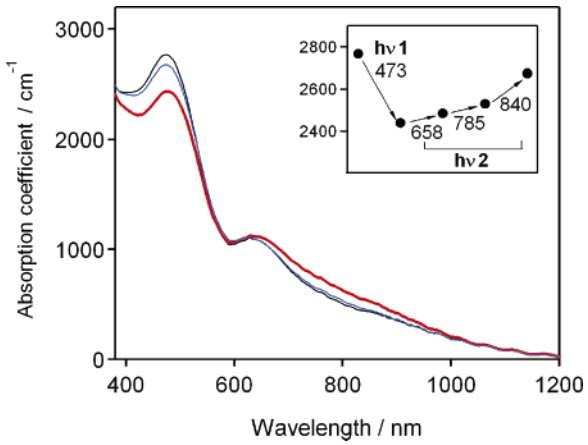

Figure 9. (a) UV−vis absorption spectra at 3 K before irradiation with light (black line), after irradiation with 473-nm light (red line), and after irradiation with 840-nm light (blue line). (Inset) The change in the intensity at 476 nm upon irradiation with 473-nm light ($h\nu_1$) and 658-, 785-, and 840-nm lights ($h\nu_2$).

close to the expected intensity ratio of $Mo^{IV}-CN-Cu^{II}$:$Mo^{IV}-CN-Cu^{I}$:$Mo^{V}-CN-Cu^{II}$ = 19:1:0.2 when the x value is 0.10. Therefore, peaks **b** and **c** are assigned to $Mo^{IV}-CN-Cu^{I}$ and $Mo^{V}-CN-Cu^{II}$, respectively, and the charge transfer from Mo^{IV} to Cu^{II} is the origin of the photoinduced change in this system.

Figure 8a shows the UV−vis absorption spectrum of a film-type of **1** and its waveform separation. The waveform separation shows that the absorption spectrum of **1** can be fitted by the following peaks: the MLCT band of $Mo^{IV} \rightarrow CN$ (250 nm),[35] the d−d transition of Mo^{IV} ($^1A_1 \rightarrow {}^1E$ (370 nm) and $^1A_1 \rightarrow {}^3E$ (400 nm)),[35] the IT band at 483 nm, and the d−d transition of Cu^{II} ($^2B_{1g} \rightarrow {}^2E_g$ (637 nm), $^2B_{1g} \rightarrow {}^2B_{2g}$ (719 nm), and $^2B_{1g} \rightarrow {}^2A_{1g}$ (855 nm)). Figure 8b,c shows the UV−vis absorption spectra after irradiation with 473-nm light (35 mW cm^{-2} for 60 min) at 3 K and the differential spectrum between 0 and 60 min irradiation, respectively. Irradiating with light causes the absorption bands of **1** to decrease and a new broad band to appear in the 600−900 nm region. The waveform separation of the differential absorption spectrum shows that this photoinduced change is explained by the decreases in the d−d transition of Mo^{IV}, the IT band, and the d−d transition of Cu^{II}, and the appearance of the band centered at 710 nm and the LMCT bands[35] of $CN \rightarrow Mo^{V}$ at 370 and 390 nm, as shown in Figure 8c. Thermal treatment to 250 K completely recovers the absorption spectrum to the original spectrum. Moreover, light reversibility is also observed; i.e., by irradiation with $h\nu_2$ light (658-, 785-, and 840-nm lights), the UV−vis absorption spectrum is almost recovered to the original spectrum (Figure 9). This indicates that the new band around 710 nm is the *reverse*-IT band from $Mo^{V}-CN-Cu^{I}$ to $Mo^{IV}-CN-Cu^{II}$.

3.2.4. Mechanism. The observed photomagnetic effect could be explained by the following. Figure 10a shows the schematic potential diagram of **1**, a class II mixed-valence compound. **1** in the initial state (state I) is paramagnetic. Irradiating with blue light ($h\nu_1$) excites **1** to the charge-transfer state (state II). Then **1** in state II immediately relaxes to state I or forms a mixed-valence isomer, $Mo^{V}-CN-Cu^{I}$ (state III). This state III is trapped at low temperature since the energy barrier is around 200 K (E_{th}). In this valence isomer state, the Mo^{V} ion ($4d^1$, S =

(35) Isci, H.; Mason, W. R. *Inorg. Chim. Acta* **2004**, *357*, 4065.

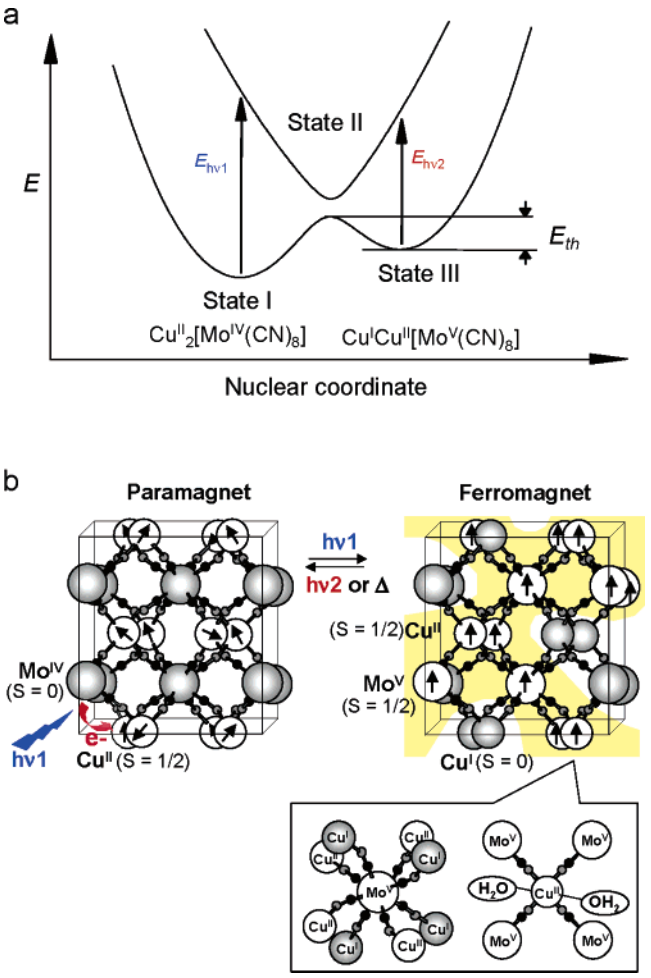

Figure 10. (a) Potential energy diagrams in the solid state of a class II mixed-valence compound. (b) Plausible schematic illustration of the irradiation-induced magnetic spin coupling in the solid state of **1**. The yellow shadow shows a possible route for the ferromagnetic spin alignment. The schematic structure is based on the crystal structure of $Mn^{II}_2[Mo^{IV}(CN)_8]\cdot 8H_2O$. The large circle is a Mo ion, the medium-size circle is a Cu ion, the small black circle is a carbon atom, and the small gray circle is a nitrogen atom.

$^1/_2$) has an unpaired electron, but Cu^I ($3d^{10}$, $S = 0$) does not. However, half of the copper ions should remain as Cu^{II} due to the stoichiometric limitations in the present compound. Therefore, the irradiated **1** is expressed as $Cu^ICu^{II}[Mo^V(CN)_8]\cdot 8H_2O$ (**1′**). Since the magnetic coupling between unpaired electrons on Cu^{II} and Mo^V in $Cu^{II}_{1.5}[Mo^V(CN)_8]\cdot 3H_2O$ is ferromagnetic,[36] the unpaired electrons on Mo^V ($S = {}^1/_2$) and Cu^{II} ($S = {}^1/_2$) of **1′** interact ferromagnetically. This is confirmed by the thermal dependence of $\chi_M T$. Figure 10b schematically shows the possible routes of the spin alignment. The schematic crystal structure in Figure 10b is proposed in the light of the obtained WAXS and EXAFS data in the present work and the reported crystal structures of analogous compounds of $M_2[Mo(CN)_8]\cdot 8H_2O$ (M = Fe, Mn). Conversely, when **1′** is irradiated by red and near-red lights ($h\nu_2$), the back electron transfer occurs via state II. Hence, **1′** returns to the original **1**. Experimentally, the photon energy (E) for the photoreduced magnetization process ($\lambda \geq 520$ nm) is lower than that for the photoinduced magnetization process ($\lambda < 520$ nm). The IT band and the *reverse*-IT band in the UV−vis absorption spectra of Figure 8 correspond to $E_{h\nu_1}$ and $E_{h\nu_2}$ in Figure 10, respectively. This result is consistent with the relationship of $E_{h\nu_2} < E_{h\nu_1}$ in the schematic potential diagram for **1**. In addition, the photostationary behavior upon irradiation by 658- and 785-nm lasers can be explained by the following: the IT band of **1** is very broad over the visible region, and hence, complex **1** slightly absorbs the 658- and 785-nm laser lights; as a result, the equilibrium between photoinduced magnetization and photoreduced magnetization is established.

4. Conclusion

We have demonstrated that the magnetic properties of a molecule-based material are reversibly switched between paramagnetic and ferromagnetic states by irradiating $Cu^{II}_2[Mo^{IV}(CN)_8]\cdot 8H_2O$ solid with visible lights. This success is due to (i) the electronic structure of class II mixed-valence compounds that meet the conditions for reversible photoinduced electron transfer and (ii) the strong exchange coupling of magnetic centers in the cyano-bridged complex. We are now investigating new Cu−Mo systems.[37−39] The objectives of our future investigations are to obtain (i) a room-temperature photomagnet, i.e., magnetic materials exhibiting photomagnetic effect at room temperature, and (ii) a single molecular photomagnet. To meet these challenges, the energy barrier (E_{th}) of the thermal back electron transfer and the T_c value in the extended network must be raised and the molecular architecture and anisotropy must be controlled.

Acknowledgment. S.O. thanks Dr. N. Machida and Mr. Y. Abe for their technical support. The present research is supported in part by a Grant for 21st Century COE Program "Human-Friendly Materials based on Chemistry" and a Grand-in-Aid for Scientific Research from the Ministry of Education, Culture, Sports, Science, and Technology of Japan. C.M. thanks Dr. J.-F. Létard for their fruitful discussions.

Supporting Information Available: Synthesis and characterization of film-type of $Cu_2[Mo(CN)_8]\cdot 8H_2O$, wide-angle X-ray scattering data, and magnetization vs external magnetic field plots. This material is available free of charge via the Internet at http://pubs.acs.org.

JA0559092

(36) To gather information on the magnetic interaction between Cu^{II} and Mo^V through the cyanide bridge, $Cu^{II}_{1.5}[Mo^V(CN)_8]\cdot 3H_2O$ (**2**) was also prepared as a reference compound. **2** is a light green powder. The field-cooled magnetization vs temperature plots for **2** in a 10 G external magnetic field show an abrupt break at 35 K. The magnetization against the external magnetic field shows that the saturation magnetization (M_S) value is 2.2 μ_B for the given formula. The observed M_S value is close to the calculated value for the parallel spin ordering of 2.5 μ_B. Hence, the magnetic coupling between Cu^{II} ($S = {}^1/_2$) and Mo^V ($S = {}^1/_2$) is ferromagnetic.

(37) Catala, L.; Mathonière, C.; Gloter, A.; Stephan, O.; Gacoin, T.; Boilot, J. P.; Mallah, T. *Chem. Commun.* **2005**, 746.
(38) Hozumi, T.; Hashimoto, K.; Ohkoshi, S. *J. Am. Chem. Soc.* **2005**, *127*, 3864.
(39) Herrera, J. M.; Marvaud, V.; Verdaguer, M.; Marrot, J.; Kalisz, M.; Mathonière, C. *Angew. Chem., Int. Ed.* **2004**, *43*, 5648.